Lab on a Chip

PAPER

View Article Online
View Journal | View Issue

Cite this: *Lab Chip*, 2018, **18**, 2433

Microfluidics within a well: an injection-molded plastic array 3D culture platform†

Younggyun Lee, ‡[a] Jin Woo Choi, ‡[b] James Yu,[c] Dohyun Park,[a] Jungmin Ha,[a] Kyungmin Son,[a] Somin Lee,[c] Minhwan Chung,[bd] Ho-Young Kim*[bd] and Noo Li Jeon*[abde]

Received 2nd April 2018,
Accepted 28th June 2018

DOI: 10.1039/c8lc00336j

rsc.li/loc

Polydimethylsiloxane (PDMS) has been widely used in fabricating microfluidic devices for prototyping and proof-of-concept experiments. Due to several material limitations, PDMS has not been widely adopted for commercial applications that require large-scale production. This paper describes a novel injection-molded plastic array 3D culture (IMPACT) platform that incorporates a microfluidic design to integrate patterned 3D cell cultures within a single 96-well (diameter = 9 mm) plate. Cell containing gels can be sequentially patterned by capillary-guided flow along the corner and narrow gaps designed within the 96-well form factor. Compared to PDMS-based hydrophobic burst valve designs, this work utilizes hydrophilic liquid guides to obtain rapid and reproducible patterned gels for co-cultures. When a liquid droplet (*i.e.* cell containing fibrin or collagen gel) is placed on a corner, spontaneous patterning is achieved within 1 second. Optimal dimensionless parameters required for successful capillary loading have been determined. To demonstrate the utility of the platform for 3D co-culture, angiogenesis experiments were performed by patterning HUVEC (human umbilical endothelial cells) and LF (lung fibroblasts) embedded in 3D fibrin gels. The angiogenic sprouts (with open lumen tip cells expressing junctional proteins) are comparable to those observed in PDMS based devices. The IMPACT device has the potential to provide a robust high-throughput experimental platform for vascularized microphysiological systems.

Introduction

Organ-on-a-chip platforms seek to model organ behaviors using *in vitro* platforms.[1,2] Such biomimetic platforms hold promise in creating an alternative method of determining human tissue-specific results for drug development without resorting to comparatively more expensive and time-consuming animal models during preclinical testing stages.[3,4] At present, new drugs require a long development period of 12 to 15 years with high rates of attrition.[5] The means of screening drug candidates for toxicity and efficacy prior to the preclinical testing phase would be crucial in eliminating a major bottleneck.[6]

Although high-throughput screening (HTS) is used extensively to streamline and scale-up drug screening through automated systems, it relies on conventional 2D cell culture platforms, which poorly mimic *in vivo* conditions.[7] As organ-on-a-chip platforms are capable of simulating complex human tissue microenvironments, the design of a microfluidics-based organ-on-a-chip device designed to incorporate a high throughput format would be advantageous in pre-clinical screening applications.[8–11]

Recent works have reported the fabrication of polymer-based microfluidic devices by injection molding,[12–15] hot embossing,[16,17] and thermoforming.[18,19] To overcome the limitations of PDMS microfluidic devices, such as small molecule absorption and low fabrication scalability,[20,21] open microfluidic platforms utilizing a geometry induced spontaneous capillary flow were introduced as a means of robust and reproducible liquid patterning.[22–24] Some of these efforts seek to increase platform accessibility by designing geometric liquid patterning inserts for pre-existing cultureware.[25]

Here, we present an injection-molded plastic array 3D culture (IMPACT) platform capable of high throughput 3D co-culture with possible applications for organ-on-a-chip

[a] *Division of WCU (World Class University) Multiscale Mechanical Design, Seoul National University, Seoul 08826, Republic of Korea. E-mail: mechlyg@gmail.com, njeon@snu.ac.kr*
[b] *Department of Mechanical and Aerospace Engineering, Seoul National University, Seoul 08826, Republic of Korea. E-mail: hyk@snu.ac.kr*
[c] *Interdisciplinary Program for Bioengineering, Seoul National University, Seoul 08826, Republic of Korea*
[d] *Seoul National University Institute of Advanced Machines and Design, Seoul 08826, Republic of Korea*
[e] *Institute of Bioengineering, Seoul National University, Seoul, Republic of Korea*
† Electronic supplementary information (ESI) available. See DOI: 10.1039/c8lc00336j
‡ These authors contributed equally to this work.

applications. This platform utilizes novel design elements incorporating structures formed within the 96-well plate format. Guiding rails formed above the base substrate across the interior walls spontaneously guide liquids (or gels containing cells) and form patterns. Using the corner and rail system, the proposed platform is capable of patterning partitioned but connected hydrogels for 3D cell co-culture applications such as angiogenesis and vasculogenesis, and delivered results equivalent to conventional PDMS microfluidics-based assays.[26,27]

This platform incorporates a mass producible injection molded polystyrene (PS) device in a 96-well plate form factor compliant design. We describe the design rule as guiding liquids from the corner to the hydrogel patterning rail such that the capillary action mediated guiding mechanism can robustly and quickly pattern multiple hydrogel structures. The IMPACT platform was used to co-culture human umbilical vein endothelial cells (HUVECs) and lung fibroblasts (LFs) in 3D fibrin gels and obtain angiogenic sprouts with structures (*i.e.* open lumen and angiogenic sprouts) and properties (*i.e.* expression of tight junction proteins) that are comparable to our previous works with PDMS devices.[28–32]

Materials and methods

Liquid movement along the corner

Corner-guided liquid transfer was observed on a 60 mm diameter PS Petri dish (contact angle, $\theta \approx 10°$, immediately after air plasma treatment) with test solutions of deionized water, 2.5 mg ml^{-1} bovine fibrinogen (Sigma) and 0.15 U ml^{-1} aprotinin (Sigma) in phosphate-buffered saline (PBS, Gibco), and 50 wt% glycerol. Test solutions were applied as droplets in 1.5, 2.0, 2.5, and 3.0 μl increments. Test liquid droplets were formed by dispensing loaded solution volumes from the pipette prior to testing surface contact, forming droplets of fixed volumes at the tip of the pipettes. The test solution droplets were then slowly lowered to the inside corner of the Petri dish. The spreading of the liquid loaded on the corner was observed using a digital microscope (AnMo Electronics, Taiwan).

Patterning performance

A prototype was fabricated using a commercially available 3D printer (EnvisionTec, Germany). The material of the device is an acrylate-based liquid photopolymer (R11) provided by the equipment manufacturer (EnvisionTec, Germany). The device was assembled using pressure sensitive adhesive (PSA) coated polycarbonate (PC) films for sealing and rendered hydrophilic with a plasma treatment (Femto Science, Korea) for 1 minute at 50 W. The movement of 3 μl of the fibrinogen solution mixed with dye loaded on the corner was recorded using a digital microscope (AnMo Electronics, Taiwan).

Device fabrication

PS injection molding was performed at R&D Factory (Korea). The aluminum alloy mold core was processed by machining and polishing (Fig. S1†). The clamping force at the time of injection was set at 130 tons with a maximum injection pressure of 55 bar, 15 seconds of cycle time, and a 220 °C nozzle temperature. A PSA coated PC film (250 μm thick) was bonded to the injection-molded PS part to complete the device (Fig. S2†).

Cell culture

Human umbilical endothelial cells, HUVECs (Lonza), were cultured in endothelial growth medium 2 (EGM-2, Lonza). Lung fibroblasts, LFs (Lonza), were cultured in fibroblast growth medium 2 (FGM-2, Lonza). The cells were incubated at 37 °C in 5% CO_2 for 3 days prior to loading. Cultured LFs and HUVECs are removed from the culture dish using 0.25% Trypsin–EDTA (Hyclone). The LFs are then re-suspended in a bovine fibrinogen solution at a cell concentration of 5×10^6 cells per ml and the HUVECs are re-suspended at a concentration of 7×10^6 cells per ml in EGM-2.

Cell patterning in the device

Before cell seeding, the device is treated for 1 minute in a plasma machine (Femto Science, Korea) with a power of 50 W. To avoid changes in hydrophilicity, experiments are performed within 30 minutes after plasma treatment. Immediately after mixing the cell-free fibrinogen solution with thrombin (0.5 U ml^{-1}, Sigma), 3 μl of the fibrin–thrombin (0.5 U ml^{-1}) solution is placed on the corner formed by the bottom and sidewalls. The liquid moves along the hydrophilic corner and move to fill two channels (depth: 0.1 mm) formed by the suspended rails, this solution is allowed to crosslink at room temperature for 4 minutes. The middle channel (MC) remains empty and becomes a closed channel with only two loading holes on the suspended beam at both ends. Immediately after mixing thrombin (0.5 U ml^{-1}) with a fibrin suspension of LFs (cell concentration of 5×10^6 cells per ml), the suspension is injected into the MC. After 4 minutes, 200 μl of the EGM-2 medium is added to the two reservoirs. The device is incubated for 18 hours at 37 °C and 5% CO_2 in an incubator. To attach HUVECs on the wall of the fibrin in the LC, after removing the media, 20 μl of EGM-2 containing the HUVECs (5×10^6 cells per ml) is loaded into the left reservoir (LR). The device is turned 90 degrees and placed in the incubator for 30 minutes so the HUVECs can settle down and form a cell sheet on the side of the fibrin gel. After attaching the HUVECs, the device is filled with EGM-2 and placed in an incubator. The medium is changed every three days.

Immunostaining

Co-cultured tissues in the device were fixed with 5% (w/v) paraformaldehyde (Biosesang, Korea) in PBS (Gibco, USA) for 15 minutes, followed by permeabilization with a 20 minute immersion in 0.15% Triton X-100 (Sigma, USA). The samples were then treated with 3% BSA (Sigma, USA) for 1 hour. Fluorescence-conjugated monoclonal mouse anti-human VE-cadherin (eBioscience, USA) and anti-human CD31

(BioLegend, USA) primary antibodies were prepared in 1 : 200 dilution and incubated overnight at 4 °C. DNA labeling was performed with a 1 : 1000 dilution of Hoechst 3342 (Molecular Probes, USA) for 1 hour at room temperature. Imaging was performed using a confocal microscope (Olympus FV1000, Japan) to produce a 3D renderable projection of the angiogenic sprouts.

Results and discussion

Fig. 1 shows a schematic of the device structure and function. The overall device is based on the form factor of a single well of a 96-well plate, but further includes a rail structure (*i.e.* "liquid guide") for patterning multiple liquids *via* capillary action, as well as a dividing wall to separate the portions above the cell culture area into two separate media reservoirs (Fig. 1a). The media reservoirs are connected through the cell culture area, allowing the generation of a chemical gradient across the patterned ECM.

Fig. 1b illustrates the structures used for liquid patterning in the IMPACT platform. The guiding corner structures exist at the intersection of the inner walls and the base substrate, while rails are formed between suspended beams (or rails) and the substrate. By design, liquid patterning begins with the application of a liquid droplet to the corner, which induces flow from the corner to the intended patterned areas through the rail structures. For the corner and rail liquid transfer mechanism to work, careful consideration is needed for dimensional and structural parameters for controlled liquid transfer.

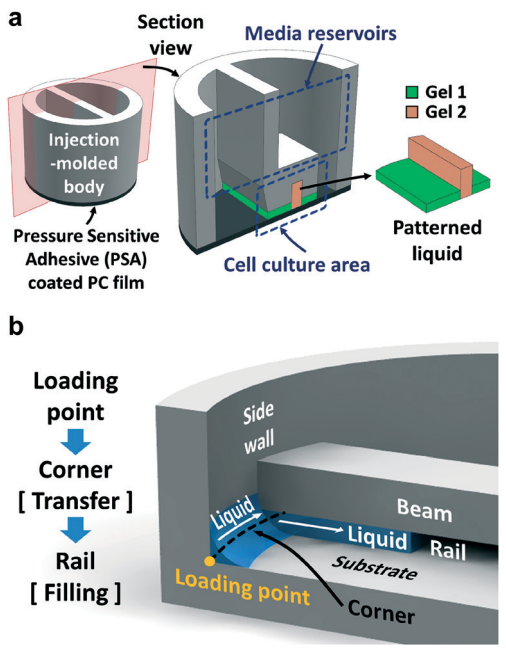

Fig. 1 Schematic of the liquid patterning mechanism. (a) A cross section of the injection molded body shows the compartmentalization of the chip into two distinct media reservoirs, connected by the cell culture area. The cell culture area utilizes capillary flow induced fluid guiding geometries to pattern up to two different types of hydrogels along the patterning rail structure. (b) A schematic illustrating the geometric guide of liquids applied to the corner, between the substrate and the side wall, to the guiding rail formed between the beam and the substrate. Post hydrophilic surface treatment, the device can spontaneously guide a liquid droplet along the corner into the liquid guide rail.

Liquid patterning

The proposed device employs a simplified system of structures within the 96-well plate format to guide and pattern liquids. Utilizing the capillary forces acting at the corners of the sidewall and the floor and with a "rail-like" gap of width, w_r, and height, h, between a closely suspended beam and the floor, liquids can be robustly and simply transferred along predetermined paths (Fig. 1b). As described, the liquid will flow along the corner by forming a wedge when the following conditions are met:[33]

$$\theta < \frac{\pi}{2} - \alpha, \tag{1}$$

which is referred to as the Concus–Finn relation. Here, θ denotes the contact angle of a given liquid on a flat substrate and α is half of the corner angle.

A scale-up version of the corner-shaped liquid patterning system using a Petri dish was used to provide a test platform for the patterning experiments (Fig. 2a). As part of the fabrication protocol, the test surface was treated with air plasma to enhance the substrate hydrophilicity, lowering the contact angle of the patterned liquid. Testing was done using DI water, the fibrinogen solution (FS), and 50 wt% aqueous glycerol (AG) in volumes ranging from 1.5 to 3.0 μl. Liquid spread distances were measured as a function of time (Fig. 2b).

As a liquid drop is deposited at the corner of a Petri dish, the capillary pressure of the drop with viscosity, μ, and surface tension, γ, causes the liquid to spread along the corner. The driving pressure gradient due to capillarity along the spreading length, l, is balanced by the gradient of viscous shear stress under negligible effects of inertia. Thus,

$$\frac{\gamma}{Rl} \sim \frac{\mu}{w_c^{\,2}} \frac{\mathrm{d}l}{\mathrm{d}t} \tag{2}$$

where R is the drop radius, corresponding to the radius of curvature to induce capillary pressure, w_c is the width of the trigonal liquid column between the corner, and $\mathrm{d}l/\mathrm{d}t$ is the spreading speed of the liquid.[34] We assume that a constant cross-sectional area is maintained throughout the length of the liquid column at any given time t,[35] and that the detailed shape of the leading meniscus is unimportant in our approximate model. Integrating relation (2), we obtain:

$$\frac{l}{R} \sim \left(\frac{w_c}{R}\right)\left(\frac{\gamma t}{\mu R}\right)^{1/2} \tag{3}$$

We can see that the length of the liquid column increases linearly with $t^{1/2}$, exhibiting a Lucas–Washburn behavior (Fig. 2c). The measured length data in Fig. 2b, for various volumes of

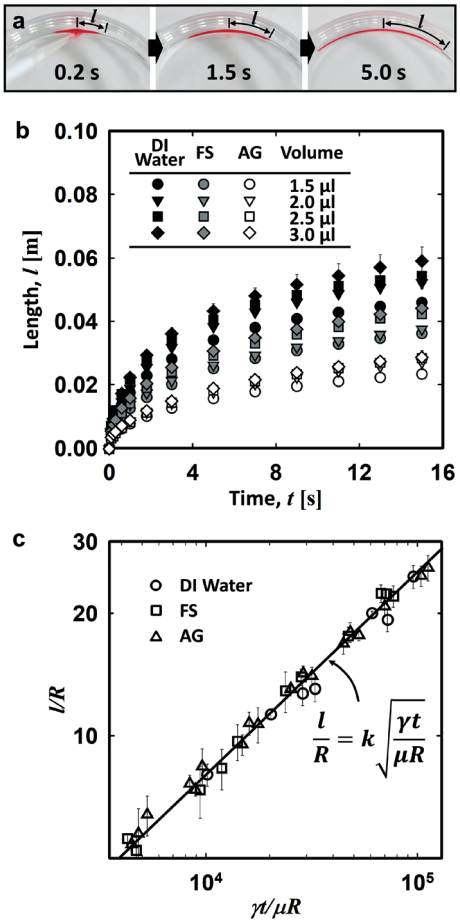

Fig. 2 Liquid patterning processes using the corner type liquid guide. (a) Time-lapse images of liquid imbibition along the corner liquid guide. (b) Plot of liquid travel distance as a function of time for the different volumes of an initial droplet (DI water = distilled water, FS = fibrinogen solution, AG = aqueous glycerol). (c) Graph of the normalized travel distance, l/R, as a function of normalized time, $\gamma t/\mu R$. The slope of the solid line, derived from the previous experiment data, is 1/2 and $k = w_c/R = 0.45$.

drops of different liquids, are fit into a single line, consistent with relation (3). Experimentally, w_c is approximately $0.45R$. The gap h between the beam and the substrate should be less than w_c for the liquid column to touch the ceiling of the rail. It is a prerequisite to the liquid transfer from the corner to the rail.

As the liquid flow is driven by the pressure gradient, the geometries of the rail and corner should be tuned to guide the flow at the corner-rail junction.[36] The pressure of the given liquid confined in the corner and the rail (Fig. 3a) is respectively given by:

$$P_c - P_a = \frac{4\gamma}{w_c}\left(\frac{\sqrt{2}}{2} - \cos\theta\right) \quad (4)$$

$$P_r - P_a = 2\gamma\left(\frac{1}{w_r} - \frac{\cos\theta}{h}\right) \quad (5)$$

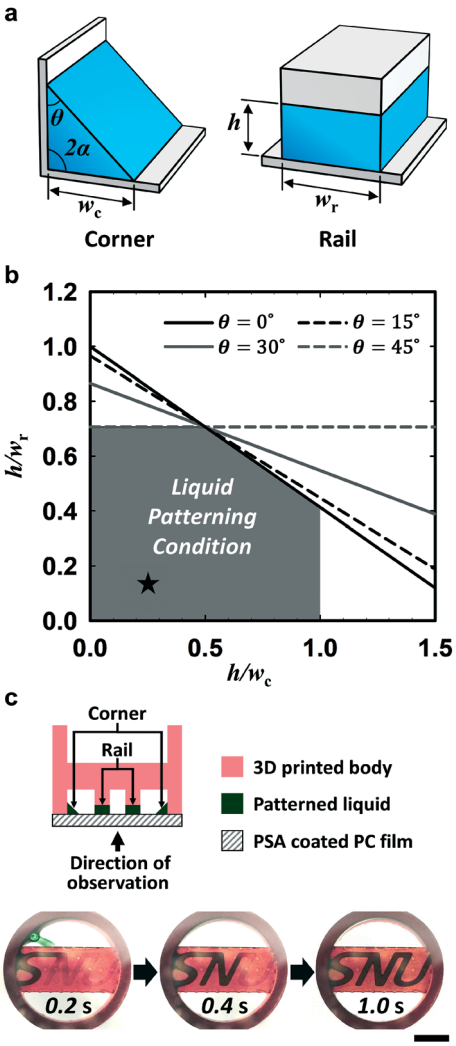

Fig. 3 Liquid patterning conditions for filling the rail. (a) The conceptual rendering of capillary filling along the corner and the rail. (b) The shaded area represents the conditions for successful liquid transfer from the corner to the rail liquid guide. (c) A 3D printed proof of concept model to pattern the liquid in the shape of "SNU". The star in Fig. 3b indicates the rail and corner dimensions of the 3D printed device, h = 0.1 mm, w_c = 0.4 mm, and w_r = 0.67 mm. A droplet of aqueous glycerol mixed with green dye (3 μl) was loaded on the corner and patterned into the "SNU" design within a second. Scale bar = 3 mm.

where P_c and P_r are the pressures of the liquid in the corner and in the rail. P_a is the atmospheric pressure. In eqn (4), the liquid cannot flow along the corner if the contact angle of the substrate is lower than $\pi/4$ and $P_c < P_a$. It coincides with the Concus–Finn relation of eqn (1). Thus, the surfaces of the PS devices are treated with plasma to induce hydrophilicity. As long as the pressure of the liquid in the corner is greater than that in the rail, the patterning liquids will always flow from the corner to the rail. This condition allows us to find the range of geometric parameters such as h/w_r and h/w_c for successful capillary filling of the rails (Fig. 3b). The theory neglects the geometry of the free surface; however, the theoretical limit driven by eqn (4) and (5) is in good agreement with

the Surface Evolver calculations in various types of corner and rail structures.[36]

We demonstrated that a droplet of aqueous glycerol (3 μl) loaded on the corner fills the rail structure within a second (Fig. 3c). Thus, selecting geometric design far from the boundaries in Fig. 3b guarantees a robust liquid patterning process. Fig. 3c shows the patterning performance of the 3D printed device in which the dimensions of the rail corresponds to the star-shaped point inside the safety regime shown in Fig. 3b. Immediately after the liquid was loaded at a point in the corner, the liquid spread along the corner and contacted the first letter "S". The capillary filling progressed along the rail path and eventually patterned the entire text "SNU" (Fig. 3c).

Device design and fabrication

Fig. 4a are photographs of the injection-molded device with labels of each functional structure and Fig. 4b illustrates the detailed dimensions of the device. A shallow channel has a depth of 0.1 mm and a width of 1.1 mm (LC). Another shallow channel has a depth of 0.1 mm and a width of 0.8 mm (RC). A relatively deeper channel with a depth of 1.5 mm and a width of 0.8 mm is located between two shallow channels (MC). All the channels lie adjacent and directly open to each other. The MC has a pair of injection holes. The star in Fig. 3b indicates the dimensions from the injection molded device (h = 0.1 mm, w_c = 0.4 mm, and w_r = 1.1 mm). The reservoir compartments are divided into a left reservoir (LR) and a right reservoir (RR), and a dividing wall is located at the LC and extends to the top of the reservoir.

The device designs were drafted in a CAD tool and used to fabricate the mold tool. After injection molding, the devices were assembled using a biocompatible adhesive film to complete the chip hardware for liquid patterning. The excellent optical performance of the PS and PC films facilitates a variety of optical observations at levels similar to those of the PDMS and glass substrates.

Fig. 4c–e show the schematics of the liquid patterning process and the photographs of each step. Liquid patterning occurs in the three distinct channels through two separate steps. Fig. 4c shows the initial empty channels. Fig. 4d depicts the channels filled in the first patterning step, wherein the left channel (LC) and the right channel (RC) are filled with acellular fibrin gel (green) while the MC is left empty. Fig. 4e illustrates the secondary loading zone in the MC (orange). As demonstrated, the liquid patterning scheme is capable of generating robust gel–gel interfaces necessary for proper cell and ECM patterning. While the primary LC and RC liquid patterning mechanism utilizes capillary action, the secondary MC patterning mainly functions on injection. The photographs at the bottom of Fig. 4c–e show the successive patterning results of the injection-molded device treated by plasma. The first loaded green liquid (3 μl of fibrinogen solution mixed with dye and thrombin) in the corner shows regularly arranged patterning areas (LC and RC). The orange liquid (fibrinogen solution mixed with orange micro-beads) injected through the inlet port of the MC forms a clear interface with the already cross-linked and immobilized fibrin matrix. The results of the optional patterning, which are driven by the dimensions set according to the design rule, are consistent with our expectations.

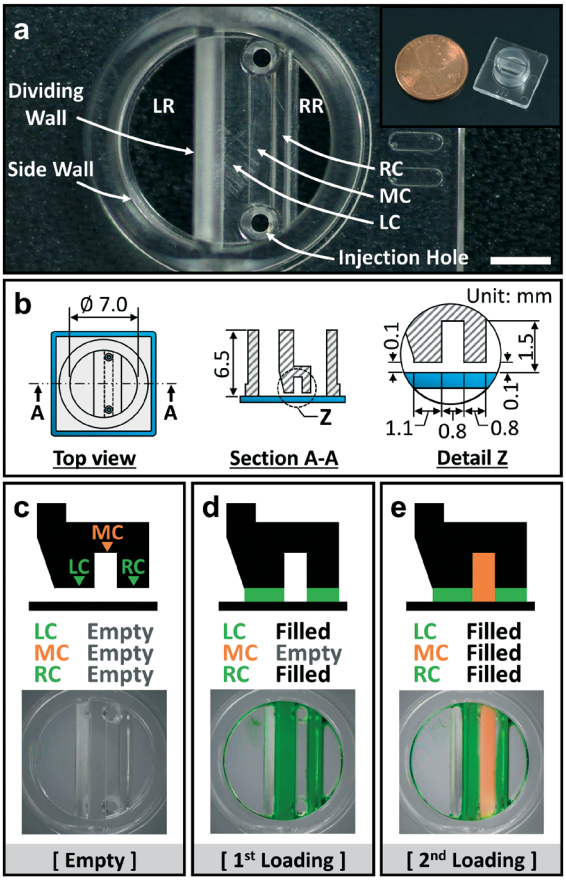

Fig. 4 Overall schematics of the structural components and liquid patterning process. (a) Top view of the injection-molded polystyrene device with labels of each component, accompanied by an isometric view of the device next to a one-cent coin. Scale bar = 2 mm. (b) Schematic view detailing the dimensions of the liquid guides. (c–e) Sequential process view for patterning two different gels in the IMPACT device. (c) The empty device prior to loading. (d) First loading, as demonstrated with green fibrin gel, occurs when the liquid is applied to the corner and spontaneously guided into both the left channel (LC) and the right channel (RC). (e) Second loading, as shown by the orange micro-beads and fibrin gel suspension, is performed by injecting the liquid into the empty middle channel (MC) through the injection hole, after the LC and RC hydrogels have cross-linked.

Compared to PDMS platforms, which are constrained by cost and difficulty to mostly single layer 2D designs, injection molding offers several advantages in terms of material compatibility, reproducibility, and manufacturability.[12,13,21] Injection molded PS, commonly used in Petri dishes, provides cell culture compatibility, low cost and a relatively long hydrophilic treatment retention time.[37–39] These advantages facilitate the successful implementation of versatile high-content 3D co-culture platforms.[40] Furthermore, injection molding

offers the freedom of design in 3D (Fig. 1). The ability to practically and economically produce three-dimensional multilevel designs allows the proposed platform to condense the previously two-dimensional PDMS device design into a PS injection-molded chip in a 96-well plate form factor. In addition, pre-existing multi-dispensing liquid handlers can be used for media transfers by arranging devices in a 96-well plate format. Such increased space efficiency and miniaturization suggest the possibility of applications in high-efficiency screening. Fig. S3† shows a 12-well IMPACT device created after redesigning into a 12-well array according to design rules. With the expectation of commercial applications requiring large scale production in the future, the device is currently in production for further development and application research.

Angiogenesis assay

Fig. 5 shows the settings and results of the angiogenesis experiment. Immediately prior to ECM arrangement, the surface of the device was exposed to plasma to induce hydrophilicity. The cell seeding configuration for the angiogenesis assay is shown in Fig. 5a. Acellular fibrin was injected into the corner, causing the fibrin solution to flow along the corner and then into the rail partition. After allowing the acellular ECM hydrogels in the LC and RC to crosslink, the MC was filled with a suspension of LF and fibrin. Following the crosslinking of the fibrin matrix in the MC, EGM-2 was loaded into medium reservoirs, and incubated overnight. On the following day, the device is voided of media *via* suctioning to prepare for HUVEC loading. A HUVEC suspension in EGM-2 is loaded into the left channel facing the media reservoir, and allowed to collect and attach to the left channel patterned region of interest (ROI) blank hydrogel surface. The media reservoirs are refilled with fresh EGM-2 and the device is incubated for the duration of the experiment, or until the EGM-2 media is changed after three days post seeding.

Fig. 5b shows the formation of tip cells and angiogenic sprouts on the second day of co-culture. Endothelial cell growth was induced and extended to the direction of LFs. After five days, angiogenic sprouts up to 0.7 mm in length were observed (Fig. 5c). Control groups wherein the LF containing gel was substituted with acellular fibrin in the MC exhibited no such sprouting. The observable sprouting in the experimental groups with an LF induced growth factor gradient, as well as the absence of sprouting in control groups without an LF induced growth factor gradient corresponds with observations on different platforms in our previous study.[31] The angiogenic sprouts exhibit the formation of vascular lumen, and immunostained imaging confirmed the presence of VE-cadherin adherens junction proteins within the sprouted vessels. Vascular lumenization is an important morphological characteristic of *in vivo* blood vessels which indicates the opening of a hollow vessel, and VE-cadherin is a commonly used marker to indicate the structural integration of endothelial cells within a vessel. The presence of both lumenization and VE-cadherin expression conditions confirm the *in vivo* like blood vessel tissue morphologies not present in 2D monolayer cultures (Fig. 5d and e). The IMPACT platform allows patterning of multiple hydrogels similar to our

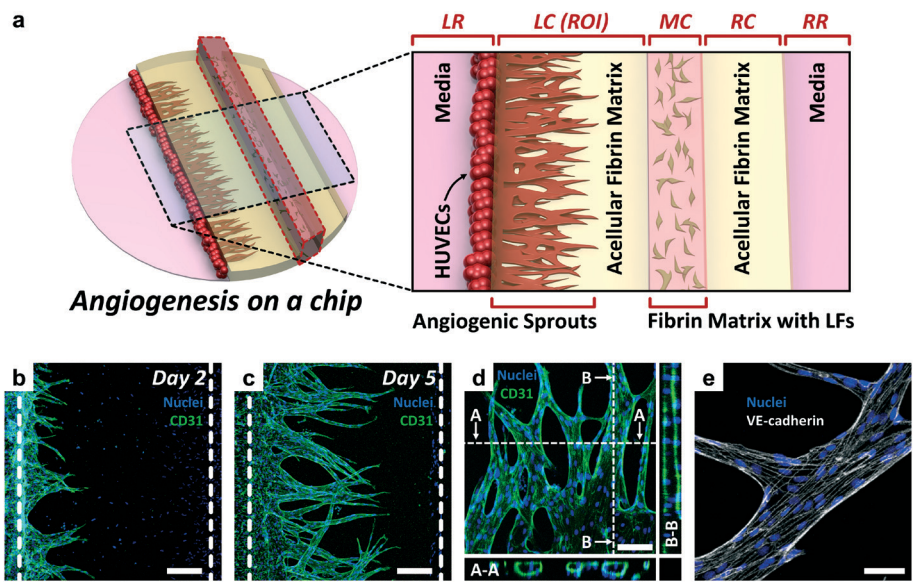

Fig. 5 Angiogenesis experiment on an IMPACT platform. (a) Cell-seeding configuration for the angiogenesis experiment. From left to right: HUVECs attached to the left side of the acellular fibrin matrix in the left channel (LC). The LFs mixed in fibrin is patterned in the middle channel (MC). Acellular fibrin in the right channel (RC). (b) Fluorescence image of the angiogenic sprout at day 2 showing endothelial tip cells invading towards the LF channel. Boundaries of the LC acellular matrix are denoted by the dotted lines. Scale bar = 200 μm. (c) Fluorescence micrograph at day 5 showing that the EC sprouts invaded about 0.7 mm. Scale bar = 200 μm. (d) Confocal cross section image of the sprouts after the day 5 clearing showing open lumen. Scale bar = 100 μm. (e) The VE-cadherin immunostained (white) image confirms the strong expression of tight junction protein VE-cadherin in the vessels. Scale bar = 50 μm.

previous PDMS device design and enables similar angiogenesis experiments on multiple similar devices at the same time.[26,30,41]

Conclusion

The application of microfluidic cell culture platforms to high-content screening requires a transition from non-standardized pilot scale PDMS devices to a mass-producible, standardized platform. Inherent material limitations render PDMS an unsuitable material for industrial scale fabrication, while injection-molded PS devices hold promise for commercial implementation.

While soft lithography based PDMS devices face difficulties in design miniaturization through multi-level designs due to challenges associated with multilevel photolithography, injection molding allows for the easy and inexpensive fabrication of three-dimensional objects. The proposed platform exploits the high design freedoms of injection molding to form a stacked configuration of the culture area and reservoir. The capillary action based liquid patterning mechanism is capable of spontaneously generating cell laden and acellular ECM hydrogel interfaces for 3D cell co-culture. The design rules presented in Fig. 3b provide a theoretical basis for the corner and rail dimensional parameters. The simple macroscale geometries utilized for capillary wetting on hydrophilic surfaces allow a streamlined and easy loading protocol, which reduces the necessary technical skills and handling time required to use the device.

Angiogenic assays using the proposed platform show comparable levels of vessel sprouting, lumenization and junction protein expression. Given the superiority of the IMPACT platform over conventional PDMS chips in terms of mass producibility, ease of use, space efficiency, high-content screening applicability, and no functional sacrifices in terms of results, the proposed platform shows promise as a large-scale replacement for PDMS devices for co-culture purposes. The proposed platform has potential applications as a versatile tool for high-content drug screening with possibilities of integration with automated liquid handlers.

Conflicts of interest

There are no conflicts of interest to declare.

Acknowledgements

We thank Ki-Cheol Park and Sang-Min Paik for their advice and assistance. This research was supported by the Basic Science Research Program and Bio & Medical Technology Development Program through the National Research Foundation of Korea (NRF) funded by the Ministry of Science, ICT, & Future Planning (NRF-2018R1A2A1A05019550, 2016R1A4A1010796, 2015M3A9D7051910).

References

1 D. Huh, G. A. Hamilton and D. E. Ingber, *Trends Cell Biol.*, 2011, **21**, 745–754.
2 D. Di Carlo, L. Y. Wu and L. P. Lee, *Lab Chip*, 2006, **6**, 1445–1449.
3 D. Huh, B. D. Matthews, A. Mammoto, M. Montoya-Zavala, H. Y. Hsin and D. E. Ingber, *Science*, 2010, **328**, 1662–1668.
4 N. S. Bhise, J. Ribas, V. Manoharan, Y. S. Zhang, A. Polini, S. Massa, M. R. Dokmeci and A. Khademhosseini, *J. Controlled Release*, 2014, **190**, 82–93.
5 J. P. Hughes, S. Rees, S. B. Kalindjian and K. L. Philpott, *Br. J. Pharmacol.*, 2011, **162**, 1239–1249.
6 E. W. Esch, A. Bahinski and D. Huh, *Nat. Rev. Drug Discovery*, 2015, **14**, 248.
7 D. Huh, Y.-S. Torisawa, G. A. Hamilton, H. J. Kim and D. E. Ingber, *Lab Chip*, 2012, **12**, 2156–2164.
8 R. P. Hertzberg and A. J. Pope, *Curr. Opin. Chem. Biol.*, 2000, **4**, 445–451.
9 L. M. Mayr and D. Bojanic, *Curr. Opin. Pharmacol.*, 2009, **9**, 580–588.
10 F. Xu, J. Wu, S. Wang, N. G. Durmus, U. A. Gurkan and U. Demirci, *Biofabrication*, 2011, **3**, 034101.
11 V. Shirure and S. George, *Lab Chip*, 2017, **17**, 681–690.
12 C. D. Chin, T. Laksanasopin, Y. K. Cheung, D. Steinmiller, V. Linder, H. Parsa, J. Wang, H. Moore, R. Rouse and G. Umviligihozo, *Nat. Med.*, 2011, **17**, 1015–1019.
13 D. A. Mair, E. Geiger, A. P. Pisano, J. M. Fréchet and F. Svec, *Lab Chip*, 2006, **6**, 1346–1354.
14 F. Deiss, A. Mazzeo, E. Hong, D. E. Ingber, R. Derda and G. M. Whitesides, *Anal. Chem.*, 2013, **85**, 8085–8094.
15 K. Metwally, T. Barriere and C. Khan-Malek, *Int. J. Adv. Manuf. Technol.*, 2016, **83**, 779–789.
16 M. Heckele, W. Bacher and K. Müller, *Microsyst. Technol.*, 1998, **4**, 122–124.
17 G. S. Fiorini, G. D. Jeffries, D. S. Lim, C. L. Kuyper and D. T. Chiu, *Lab Chip*, 2003, **3**, 158–163.
18 E. J. Vrij, S. Espinoza, M. Heilig, A. Kolew, M. Schneider, C. Van Blitterswijk, R. Truckenmüller and N. C. Rivron, *Lab Chip*, 2016, **16**, 734–742.
19 R. Truckenmüller, S. Giselbrecht, N. Rivron, E. Gottwald, V. Saile, A. Van den Berg, M. Wessling and C. Van Blitterswijk, *Adv. Mater.*, 2011, **23**, 1311–1329.
20 M. W. Toepke and D. J. Beebe, *Lab Chip*, 2006, **6**, 1484–1486.
21 E. Berthier, E. W. Young and D. Beebe, *Lab Chip*, 2012, **12**, 1224–1237.
22 S. H. Lee, A. J. Heinz, S. Shin, Y. G. Jung, S. E. Choi, W. Park, J. H. Roe and S. Kwon, *Anal. Chem.*, 2010, **82**, 2900–2906.
23 B. P. Casavant, E. Berthier, A. B. Theberge, J. Berthier, S. I. Montanez-Sauri, L. L. Bischel, K. Brakke, C. J. Hedman, W. Bushman, N. P. Keller and D. J. Beebe, *Proc. Natl. Acad. Sci. U. S. A.*, 2013, **110**, 10111–10116.
24 J. Berthier, K. A. Brakke and E. Berthier, *Open microfluidics*, John Wiley & Sons, 2016.
25 S. B. Berry, T. Zhang, J. H. Day, X. Su, I. Z. Wilson, E. Berthier and A. B. Theberge, *Lab Chip*, 2017, **17**, 4253–4264.
26 C. P. Huang, J. Lu, H. Seon, A. P. Lee, L. A. Flanagan, H.-Y. Kim, A. J. Putnam and N. L. Jeon, *Lab Chip*, 2009, **9**, 1740–1748.

27 S. Kim, H. Lee, M. Chung and N. L. Jeon, *Lab Chip*, 2013, **13**, 1489–1500.
28 H. Lee, W. Park, H. Ryu and N. L. Jeon, *Biomicrofluidics*, 2014, **8**, 054102.
29 M. Kang, W. Park, S. Na, S. M. Paik, H. Lee, J. W. Park, H. Y. Kim and N. L. Jeon, *Small*, 2015, **11**, 2789–2797.
30 S. Kim, M. Chung and N. L. Jeon, *Biomaterials*, 2016, **78**, 115–128.
31 S. Kim, M. Chung, J. Ahn, S. Lee and N. L. Jeon, *Lab Chip*, 2016, **16**, 4189–4199.
32 M. Chung, J. Ahn, K. Son, S. Kim and N. L. Jeon, *Adv. Healthcare Mater.*, 2017, **6**, 1700196.
33 P. Concus and R. Finn, *Proc. Natl. Acad. Sci. U. S. A.*, 1969, **63**, 292.
34 A. Ponomarenko, D. Quéré and C. Clanet, *J. Fluid Mech.*, 2011, **666**, 146–154.
35 M. M. Weislogel, J. A. Baker and R. M. Jenson, *J. Fluid Mech.*, 2011, **685**, 271–305.
36 J. Berthier and K. A. Brakke, *The physics of microdroplets*, John Wiley & Sons, 2012.
37 H. Ohishi, S. Kishimoto and T. Nishi, *J. Appl. Polym. Sci.*, 2000, **78**, 953–961.
38 R. France and R. Short, *J. Chem. Soc., Faraday Trans.*, 1997, **93**, 3173–3178.
39 P. M. van Midwoud, A. Janse, M. T. Merema, G. M. Groothuis and E. Verpoorte, *Anal. Chem.*, 2012, **84**, 3938–3944.
40 Y.-C. Tung, A. Y. Hsiao, S. G. Allen, Y.-S. Torisawa, M. Ho and S. Takayama, *Analyst*, 2011, **136**, 473–478.
41 B. Mosadegh, C. Huang, J. W. Park, H. S. Shin, B. G. Chung, S.-K. Hwang, K.-H. Lee, H. J. Kim, J. Brody and N. L. Jeon, *Langmuir*, 2007, **23**, 10910–10912.